Pre-rRNA represses gene transcription in the XY body of male germ cells

Linlin Chen[1,2], Xiaochen Gai[1,2], Si Chen[1,2], Qilin Li[1,2], Yifan Sun[3], Peng Li[3], Chencheng Yao[3], and Xiaochun Yu[1,2]*

[1]State Key Laboratory of Gene Expression, School of Life Sciences, Westlake University, Hangzhou, Zhejiang, China.

[2]Westlake Laboratory of Life Sciences and Biomedicine, Hangzhou, Zhejiang, China.

[3]Department of Andrology, Center for Men's Health, Department of ART, Institute of Urology, Urologic Medical Center, Shanghai Key Laboratory of Reproductive Medicine, Shanghai General Hospital, Shanghai Jiao Tong University School of Medicine, Shanghai, China.

L.C. and X.G. contribute equally to this work

*To whom correspondence should be addressed. Email: yuxiaochun@westlake.edu.cn

Running title: Pre-rRNA mediates MSCI

Keywords: nucleolus, pre-rRNA, the XY body, meiosis, gene transcription

Abstract

Nucleolus is disassembled when the nuclear envelope breaks down during mitosis prophase. However, the dynamics of nucleolus in meiotic prophase remain unclear. Here, by tracking nucleolar components, we show that nucleolus is fragmented even before the breakdown of the nuclear envelope. Instead of dissolving in nucleoplasm or cytoplasm, the nucleolar components are reaggregated and fuse with the XY body during the prophase I of meiosis. The dynamic relocation of the nucleolar components to the XY body is governed by the ATR-dependent signaling pathway. Moreover, the relocated pre-rRNA covers the entire X and Y chromosomes. The treatment with RNA polymerase I inhibitor BMH-21 only disrupts the accumulation of pre-ribosomal RNA (pre-rRNA) but not other nucleolar components on the X and Y chromosomes. Surprisingly, this disruption of pre-rRNA induces the recruitment of RNA polymerase II to the XY body and partially abolishes meiotic sex chromosome inactivation (MSCI). Taken together, this study reveals pre-rRNA as a key epigenetic regulator for MSCI.

Significance statement

Both nucleolus and the XY body are nuclear membraneless condensates. In this study, we show that nucleoli fuse with the XY body during the prophase I of meiosis in the male germ cells, providing the evidence that two different nuclear bodies fuse together in a dynamic process. Moreover, associated with the fusion, pre-rRNA relocates onto the X and Y chromosomes, acting as non-coding RNA to occupy gene regions and represses gene transcription in the sex chromosomes. Thus, this study reveals that the products from RNA polymerase I-meditated transcription repress RNA polymerase II-meditated gene transcription.

Introduction

The nucleolus is a nuclear membraneless organelle serving as the hub for ribosomal RNA (rRNA) transcription, processing, and ribosome assembly[1–6]. Structurally, the nucleolus exhibits a tripartite architecture comprising the fibrillar center (FC), the dense fibrillar component (DFC), and the granular component (GC)[6–8]. FC is the innermost layer where RNA polymerase I (pol I) mediates pre-rRNA transcription. DFC is the middle layer where the newly synthesized pre-rRNA is modified and processed. GC is the outer layer where the ribosomal protein subunits are integrated into rRNA to form the small and large ribosomal subunit precursors (pre-60S and pre-40S)[9–11]. These precursors are eventually shipped to cytoplasm to assemble mature ribosomes for protein translation.

The nucleolus continues generating pre-ribosomal particles during the interphase[12]. However, during mitosis, the nucleolus is disassembled, and ribosomal biogenesis is halted. When nuclear envelope breaks down during mitotic prophase, nucleolus is fragmented and dissolved[13–15]. Early studies show that residual transcription machinery and pre-rRNA were kept at rDNA loci during mitosis, and nucleolus is reformed upon nuclear envelope assembly[14]. Recently, with advanced microscopy, we and others have revealed that nucleolar components, including pre-rRNA, cover condensed chromosomes during mitosis to avoid the clustering of the condensed chromosomes before segregation[16,17].

Different from mitosis, meiosis has an extended prophase I before the first round of cell division, especially for male germ cells[18,19]. The prolonged prophase I in male germ cells can be further divided into five stages, namely leptotene, zygotene, pachytene, diplotene, and diakinesis, during which homologous chromosomes are aligned together and associated with the synaptonemal complex (SC)[20–23]. SPO11, a

topoisomerase-like enzyme, generates DNA double-strand breaks (DSBs) on homologous chromosomes to initiate meiotic recombination[24–27]. And these DSBs are ultimately repaired by homologous recombination repair machinery during meiotic prophase I[28–30].

However, the male germ cells have two different sex chromosomes, the X and Y chromosomes. These two chromosomes share homology only at the subtelomeric region, thus forming synapses only in the subtelomeric region[31–34]. Interestingly, these two sex chromosomes are conjugated together, forming the XY body, a membraneless nuclear body from pachytene to diplotene[35,36]. While RNA polymerase II (pol II)-mediated gene transcription is activated on autosomes during meiotic prophase I, gene transcription is silenced in the XY body, known as meiotic sex chromosome inactivation (MSCI)[37–39]. Consistently, pol II is specifically excluded from the XY body, although the underlying mechanism remains elusive[40]. Moreover, due to lacking homologous templates, the repair of SPO11-mediated DSBs is prolonged in the XY body. And numerous DNA damage response factors are enriched in the XY body[41,42]. A typical example is the ATR-dependent phosphorylation of histone H2AX (aka γH2AX), also acting as the surrogate marker for the XY body[43–47].

In this study, we tracked the dynamic changes of nucleolus in meiotic prophase I and found that nucleolus was fused with the XY body. Pre-rRNA covers on the X and Y chromosomes and mediates MSCI.

Results

Nucleolus disassembles in the pre-leptotene spermatocytes

To investigate the dynamic regulation of nucleolus in meiotic prophase of male germ cells, we tracked the localization of pre-rRNA, the major component in the nucleolus[48]. First, we examined the transition from the c-Kit-positive differentiating spermatogonia to pre-leptotene spermatocytes, which represents the transition from the final interphase to meiotic prophase I. Using fluorescence in situ hybridization (FISH)[49], we observed that pre-rRNA clearly formed condensates in the c-Kit-positive differentiating spermatogonia, suggesting that nucleoli are intact in the final interphase prior to meiosis (Figure 1A). However, in pre-leptotene, pre-rRNA became diffused in the nucleoplasm and was occasionally observed in discrete granules, suggesting that nucleoli start disassembly upon entry into pre-leptotene (Figure 1A).

Since nucleolus has three different layers, we examined the integrity of FC, DFC, and GC with different biomarkers including POLR1E for FC, FBL for DFC, and NPM1 for GC[48,50]. Consistently, all three compartments exhibited widespread dispersion throughout the nucleoplasm in the pre-leptotene spermatocytes (Figure 1B, Figure S1). Of note, compared to FC and DFC, pre-rRNA and GC diffused into a larger area (Figure 1A and 1B, Figure S1), indicating that pre-rRNA may largely associate with GC components during the nucleolar disassembly.

To further explore the nucleolus disassembly, we performed 5-ethynyl uridine (5-EU) incorporation assays. As 80-90 % nascent RNA is pre-rRNA, transient incorporation of 5-EU mainly labels pre-rRNA[48,51,52]. As expected, 5-EU was incorporated into pre-rRNA in nucleoli of c-Kit-positive spermatogonia (Figure 1C). In sharp contrast, 5-EU incorporation into pre-rRNA was largely suppressed in pre-leptotene spermatocytes (Figure 1C), suggesting that pol I-mediated pre-rRNA

transcription is arrested when nucleoli start disassembly. Collectively, the nucleolus loses the tripartite architecture and the capability to synthesize pre-rRNA in the pre-leptotene spermatocytes (Figure 1D).

Nucleolar components dynamically fuse with the XY body

Next, we isolated spermatogenic cells from leptotene to diplotene using fluorescence-activated cell sorting (FACS)[53,54], and analyzed the dynamic reorganization of nucleolar components in meiotic prophase I. At the leptotene stage, pre-rRNA and NPM1 appeared in many dispersed granules with different sizes, which began to coalesce as cells progressed into zygotene (Fig. 2A and 2B). Upon entry into pachytene, coinciding with the formation of the XY body, we observed a striking spatial reorganization as both pre-rRNA and NPM1 were progressively recruited towards and subsequently sequestered in the XY body (Figure 2A and 2B). Quantitative analysis of signal intensity of pre-rRNA and NPM1 reveals a gradual accumulation of both components in the XY body from early pachytene to diplotene (Figure 2A and 2B). By late pachytene, pre-rRNA and NPM1 fully localized in the XY body (Figure 2A and 2B). Moreover, ChIRP-seq analyses of pre-rRNA and CUT＆Tag-seq analyses of NPM1 show that the enrichment of pre-rRNA and NPM1 was strictly confined to the X and Y chromosomes, but not on autosomes (Figure 2C). In addition, other nucleolar components, such as POLR1E and FBL, showed similar dynamic relocation to the XY body during prophase I (Figure S2). Collectively, following nucleolar disassembly, the nucleolar components are reaggregated and fused into the XY body during meiotic prophase I (Figure S3).

Moreover, different from nucleolar disassembly in mitotic prophase, the fusion of nucleolus and the XY body occurs when the nuclear envelope remains structurally

intact throughout the pachytene stage (Figure S4A). In addition, we examined and found that the rDNA loci remained spatially distinct and were not overlapped with the XY body (Figure S4B), further confirming that nucleolus organizing regions (NORs) are disassembled, and the nucleolar components are disassociated from the rDNA loci and fused with the XY body.

ATR-mediated DNA damage response signaling drives the sequestration of nucleolar components to the XY body.

During the meiotic prophase I, the delayed repair of programmed DSBs on the unsynapsed X and Y chromosomes triggers a localized DNA damage response, which is mediated by ATR-dependent γH2AX[55–59], also acting as a surrogate marker of the XY body. Here, we examined whether the recruitment of nucleolar components to the XY body is dependent on DNA damage response. We isolated pachytene spermatocytes and treated them with the specific ATR inhibitor AZ20 for 24 hours to ablate DDR[60] (Figure 3A). While γH2AX was abolished in response to the ATR inhibitor treatment, HR repair factors including RAD51 and BRCA1 localized at the unsynapsed region of the X and Y chromosomes (Figure S5A). Moreover, we did not observe obvious changes on the morphology of the XY body (Figure S5A). Interestingly, we found that along with the disruption of γH2AX, both pre-rRNA and NPM1 were released from the XY body (Figure 3A and 3B). γH2AX started to be enriched at the unsynapsed region of the X and Y chromosomes one hour after the ATR inhibitor was washed away, and its localization in the XY body was fully recovered four hours after the treatment was removed. Again, the localization of both pre-rRNA and NPM1 was restored along with the recovery of γH2AX (Figure 3A and 3B), suggesting that the fusion of nucleolar components with the XY body is dependent on the DNA damage response signals.

It has been shown that genetically knocking out the *H2ax* gene abolished the formation of the XY body as well as the synapsis between these two sex chromosomes. However, both RAD51 and BRCA1 remained on the elongated X chromosome in pachytene (Figure S5C and S5D), suggesting that SPO11 still mediates DSBs on the X chromosome even in the absence of H2AX. However, neither pre-rRNA nor NPM1 existed on the X and Y chromosomes (Figure 3C). Thus, these results suggest that DSBs pe se are not important for the recruitment of the nucleolar components to the XY body. Instead, it is the DNA damage response signals mediating the recruitment of the nucleolar components.

Pre-rRNA mediates MSCI

Since nucleolar components cover the transcriptionally silenced sex chromosomes, we wonder if nucleolar components may contribute to MSCI. To test this hypothesis, we treated spermatocytes with pol I inhibitor BMH-21[61]. BMH-21 recognizes GC-rich sequences not only to block pol I binding to the promoter regions of rDNA but also to remove pre-rRNA from chromatin. Thus, BMH-21 treatment quickly released pre-rRNA from the XY body without affecting spermatocyte viability (Figure S6A-S6C). However, the transient treatment did not affect the localization of NPM1 in the XY body (Figure S7A), suggesting that rRNA species and nucleolar proteins may recognize different binding partners in the XY body. Moreover, exposure to 2.5 μM BMH-21 for 12 hours affected neither γH2AX in the XY body (Figure S7B), allowing us to assess the specific consequence of loss of pre-rRNA in transcription regulation on the sex chromosomes.

We then monitored transcriptional activity in the XY body using 5-EU labeling. In control pachytene spermatocytes, the XY body is devoid of nascent RNA because of

MSCI (Figure 4A). Strikingly, upon exclusion of pre-rRNA from the XY body by BMH-21, we observed the accumulation of 5-EU-labeled nascent RNA species in the XY body, indicating a failure of MSCI (Figure 4A). To quantitatively examine the transcriptional reactivation, we isolated spermatocytes at the pachytene stage and treated the cells with BMH-21 (Figure 4B). We found that the overall gene expression on the X and Y chromosomes was significantly higher than that on autosomes (Figure 4B). Detailed transcriptomic profiling reveals that 237 X-linked genes and 9 Y-linked genes were significantly upregulated ($\geqslant$ 2-fold change, $P_{adj} < 0.05$) (Figure 4C), confirming the specific transcription regulation by pre-rRNA. Moreover, we randomly selected representative X-linked genes (*Pabir2, Dmd, Xlr, Ccnb3*) and Y-linked genes (*Uty, Usp9y, Zfy2*), and performed gene-specific qPCR to validate the RNA-sequencing results (Figure 4D).

Because MSCI failure causes complete arrest and elimination of male germ cells at the pachytene stage of meiotic prophase I[37], we next tested whether pre-rRNA inhibition could phenocopy this defect *in vivo*. To disrupt pre-rRNA localization within the XY body, BMH-21 was delivered to spermatocytes by rete testis microinjection in 8-week-old male mice (Figure S8A). One week after injection, BMH-21-treated testes were markedly atrophic (Figure S8B). Loss of round spermatid and PNA-positive cells indicated that BMH-21 treatment may cause defects at or before meiosis (Figure S8C and 8D). The presence of only a few pachytene spermatocytes further suggested that spermatocytes might be eliminated at or after the pachytene stage (Figure S8C and 8D). These results indicate that proper pre-rRNA localization within the XY body is required for meiosis.

Taken together, these results demonstrate that pre-rRNA is indispensable for maintaining MSCI in the XY body.

Pre-rRNA mediates the exclusion of RNA Polymerase II from the XY body

Under normal physiological conditions, the execution of MSCI requires the rigorous exclusion of RNA Polymerase II (Pol II) from the XY chromatin territory[60,62]. Given the specific accumulation of pre-rRNA within this silent compartment, we hypothesized that pre-rRNA might play a role in restricting Pol II access. To test the hypothesis, we depleted pre-rRNA using BMH-21 and monitored Pol II localization. Strikingly, upon loss of pre-rRNA, we observed the relocation of Pol II in the XY body (Figure 5A). These results imply that the presence of pre-rRNA is essential to enforce the exclusion of Pol II from the sex chromosomes.

To substantiate the aforementioned spatial antagonism at the genomic level, we performed correlative ChIRP-seq (for pre-rRNA) and CUT&Tag (for Pol II) (Figure 5B). The sequencing data reveal a robust inverse correlation between pre-rRNA occupancy and Pol II binding. Specifically, BMH-21 treatment caused a marked reduction of pre-rRNA on the sex chromosomes, which was mirrored by a concomitant increase in Pol II occupancy across the XY chromatin (Figure 5B). Genome-wide peak analyses further confirm that pre-rRNA occupancy in the XY body coincides with the transcriptional suppression of Pol II targets (Figure 5C). Conversely, the depletion of pre-rRNA led to Pol II recruitment at specific loci of MSCI, such as *Dmd*, *Ccnb3,* and *Zic3* (Figure 5D). Collectively, these results suggest that pre-rRNA functions as a critical spatial regulator that physically excludes Pol II from the XY chromatin, thereby maintaining the transcriptional silencing of the sex chromosomes in meiotic prophase.

Pre-rRNA enforces a repressive chromatin state in the XY body

Long noncoding RNAs (lncRNAs) are emerging as key architects of chromatin organization that modulate transcriptional outputs[63–65]. Given the accumulation of pre-rRNA in the XY body, we asked whether the pre-rRNA regulates the accessibility of sex chromosomes to maintain MSCI. To verify this hypothesis, we assessed genome-wide chromatin accessibility changes upon pre-rRNA depletion. Pachytene spermatocytes were isolated and subjected to ATAC-seq (Figure 6A). Compared to the autosomes, the mean chromatin accessibility of the X chromosome (with 1.61-fold) and the Y chromosome (with 1.53-fold) was increased in response to the BMH-21 treatment (Figure 6A). The metagene and heatmap analyses demonstrate that BMH-21-induced expansion of open chromatin specifically across the sex chromosomes (Figure 6B and 6C). According to the peak calling, we found 1020 genes on the sex chromosomes that exhibited significantly gained accessibility (Figure 6D). To link this structural relaxation directly to pre-rRNA occupancy, we integrated these ATAC-seq data with our ChIRP-seq profiles. Notably, we found a high degree of overlap on 397 of these genes (84.47% of the analyzed subset) corresponding to genomic regions that lost pre-rRNA occupancy upon BMH-21 treatment (Figure 6E). Collectively, these results indicate that pre-rRNA limits chromatin accessibility of the XY chromatin, acting as a molecular barrier to maintain MSCI (Figure 6F).

Discussion

In this study, we have shown that nucleolus is disassembled in pre-leptotene. The nucleolar components are reaggregated in leptotene/zygotene and fuse with the XY body in pachytene/diplotene. This dynamic regulation of nucleolus is unique in meiotic prophase I. In mitosis prophase, nucleolus disassembly is associated with nuclear envelope breakdown. However, from pre-leptotene to diplotene, nuclear envelope is intact, suggesting that special signals associate with homologous chromosome packing and alignment may induce nucleolus disassembly in meiotic prophase I.

A more striking observation is that nucleolar components are reaggregated and fuse into the XY body. Like nucleolus, the XY body is a membraneless nuclear body[37]. Here, we have shown that two different types nuclear bodies fused together. Homogeneous fusion of liquid-liquid phase separation is commonly observed along with the increased level of condensate materials[66]. However, heterogenous condensates fusion is rare to be observed. Currently, the underlying mechanism driving the fusion of nucleolus and the XY body remains elusive. Nevertheless, we have shown that the fusion is dependent on the ATR-mediated signals as ATR inhibitor treatment abolishes the retention of pre-rRNA and NPM1 in the XY body. Moreover, pre-rRNA and NPM1 relocate back to the XY body following removal of ATR inhibitor. Our earlier studies have shown that MDC1, a functional and binding partner of γH2AX in DNA damage response, recognizes pre-rRNA[49]. It is likely that MDC1 targets pre-rRNA to the XY body. However, pre-rRNA can also be released by the treatment of BMH-21, a G/C rich sequence binder, suggesting that once pre-rRNA enters into the XY body, it is associated with genomic DNA. Thus, it is possible that following the recruitment by MDC1, pre-rRNA expends onto the chromatin, which mimics the expansion of XIST on chromatin during the X chromosome inactivation.

In fact, similar to the role of XIST in transcription repression[67–69], pre-rRNA silences gene transcription in the XY body by repelling pol II. Based on our observation, we propose that pre-rRNA physically occupies the XY chromatin and blocks the pol II assessment to gene elements. Thus, pre-rRNA-mediated gene silencing may share the similar mechanism conducted by XIST during the X chromosome inactivation.

Pre-rRNA is the raw material to be processed into mature rRNA for ribosome assembly[70]. Here, we show the evidence that pre-rRNA has been repurposed for gene silencing as non-coding RNA during meiotic prophase I. Moreover, our earlier study reveals that pre-rRNA may participate in HR repair for DSBs in the XY body[49]. Thus, the collective evidence suggests the multiple roles of pre-rRNA during different biological processes.

In addition to pre-rRNA, other nucleolar components, including protein components, are also fused into the XY body. Such relocations are also mediated by the ATR-dependent signaling pathway. Like pre-rRNA, these protein components, such as NPM1, are also enriched on the chromatin. However, BMH-21 treatment did not release NPM1 from the XY body, suggesting that once NPM1 enters the XY body, it may recognize specific partners. The biological functions of these nucleolar proteins in the XY body need to be examined in future. Of note, FBL, a methyltransferase catalyzing 2'-O-methylation on pre-rRNA[6], is specifically enriched on the unsynapsed axis of the X and Y chromosome, where SPO11-mediated DSBs occur. Thus, it is possible that these nucleolar proteins may be involved in meiosis-related events in the XY body, such as meiotic DSB repair. And we do not exclude the possibility that these nucleolar proteins also participate in MSCI.

In our study, we also notice that loss of γH2AX in the XY body by the ATR inhibitor treatment does not abolish the structure of the XY body. However, the XY

body cannot form in the *H2ax* gene knock-out mice. It is possible that γH2AX mediates the priming of the XY body formation. Once the XY body is established, gH2AX is indispensable for the structural integrity of the XY body[71]. Similarly, the γH2AX/MDC1 mediates the recruitment of pre-rRNA to the XY body. Once pre-rRNA gets into the XY body, it starts to expand onto the chromatin. However, we currently cannot exclude that the structural role other than the phosphorylation on Ser139 of H2AX is important for the XY body formation.

In conclusion, this study delineates an unexpected link between nucleolus and the XY body, two different nuclear bodies. We propose that the programmed disassembly of the nucleolus and the subsequent repurposing of pre-rRNA maintain the epigenetic silence of the X and Y chromosomes in meiotic prophase I.

Materials and methods

Mice

All mice experiments were permitted by Westlake University Animal Care and Use Committee and were performed according to the approved protocol. For all experiments, C57BL/6J mice were used, except where otherwise specified. Wild-type mice were obtained from Westlake University Animal Center. *H2AX*$^{+/-}$ mice were gifted from Linyu Lu (Zhejiang University). To generate gene knockout mice, heterozygous mating produces offspring. Spermatocytes were obtained from 3 to 4-week-old mice. All mice were housed in specific-pathogen-free conditions at ~22 °C with a humidity range of 40%–70% and a 12-hour light/dark cycle.

Collection and culture of spermatocytes

Previously established method for short-term culture were performed (Hironori Abe et al., 2022). Briefly, testes were collected from 3 to 4-week-old C57BL/6J mice. Then the tunica albuginea was removed. The decapsulated testes were minced with a micro-dissecting scissor. Transferred them into 2mL of Minimum Essential Medium alpha (Gibco, 12000-022) and incubated for 15 min at 35°C with 1 mg/ml collagenase (type IV, ThermoFisher) and 20 U DNase I (Vazyme, EN401). After that, the cells were centrifuged to discard the supernatant. The remaining seminiferous tubules were digested by TrypLE™ Express (Gibco, 12604021) with 50 U DNase I and 2 mg/ml collagenase IV for 10 minutes at 35°C. The digestion was terminated by MEMα with 5% FBS. The single-cell suspension was centrifuged at 500g for 3 minutes and washed three times with MEMα. Filter cells into a 50 mL tube through a 40 μm cell strainer (Falcon, 352340). The cells were collected and cultured in MEMα.

For drug treatment experiments, the collected cells were cultured in MEMα

containing DMSO (control), BMH-21 (Selleck, S7718), or AZ20 (Selleck, S7050). For recovery experiments, the control and treated cells were washed three times and collected by centrifugation at 500g for 3 minutes after drug incubation. For ionizing radiation-induced DNA damage in meiosis, cells were treated with 10 Gy of X-ray. After 4 hours of recovery, the cells were collected for the next experiments.

Meiotic chromosome spreads

Meiotic chromosome spread slides were prepared as previously described[72]. Some details and conditions were modified. For the fresh tissue, testes were excised from mice. The tunica albuginea was removed. Put the seminiferous tubules in phosphate-buffered saline (PBS). Each testis was transferred to 1 mL PBS and gently unraveled with tweezers. Then, the seminiferous tubules were transferred to a hypotonic extraction buffer (30 mM Tris-HCl, 50 mM sucrose, 17 mM sodium citrate, 5 mM EDTA, 0.5 mM dithiothreitol, and 0.1 mM phenylmethylsulfonyl fluoride) for further processing. After incubation on ice for 10 minutes, the same volume of sucrose (100 mM) was added to the hypotonic extraction buffer. Seminiferous tubules were mashed with tweezers and pipetted up and down several times. The suspension was filtered by a 70 μm cell strainer (Corning, 431751). After that, the slides were soaked in fixation buffer (1% paraformaldehyde, 0.1% TritonX-100, pH 8.2) for several minutes. Take the slides out and keep them flat. The 100 μL suspension was added to the slides. A slight movement spreads the suspension and fixation buffer over the entire slide. The slides were placed in humidified chambers at room temperature and air-dried overnight. The meiotic chromosome spread slides were stored in slide boxes at −80°C.

Immunofluorescence (IF) and RNA fluorescence in situ hybridization (FISH)

The chromosome spread slides were washed three times in PBS. Then, cells were blocked for 30 minutes at room temperature in PBS containing 3% bovine serum albumin (BSA). After that, cells were incubated with 200 μL dilution of primary antibodies in 1% bovine serum albumin at 4 ℃ overnight. The slides were washed three times in PBS with 0.1% Tween 20 and then incubated for 2 hours with secondary Antibodies at room temperature. After washing three times, DNA was counterstained with DAPI.

For FISH, slides were performed as described previously[73]. Cells were washed in PBS and dehydrated using 70%, 80%, and then 100% ethanol for 2 minutes each, followed by air-drying until completely dry. Then, cells were first incubated with wash buffer I (SMF-WA1-60, Bioresearch technologies) for 10 minutes at room temperature. The RNA probes were diluted with hybridization buffer (SMF-HB1-10, Bioresearch Technologies). The chromosome spreads were incubated with diluted probe solution, gently covered with Parafilm. The slides were put in a humidified chamber at 37°C overnight. The next day, Parafilm was removed, and slides were incubated with the same wash buffer I for 20 minutes at room temperature. The slides were washed with PBS and counterstained with DAPI. The pre-rRNA probes were used in the previous study[49].

For RNA fluorescence in situ hybridization and combined immunofluorescence experiment, the slides were fixed with 4% paraformaldehyde (PFA) after the secondary antibody incubation. Then, FISH was performed as described.

All of the images were obtained with Zeiss LSM900 confocal microscope equipped with a 63x/1.4 oil lens (Zeiss), and were processed using ImageJ.

Fluorescence-activated cell sorting (FACS)

Sub-populations of spermatogenic cells and spermatocytes were isolated from mice following a published protocol[53,54]. Briefly, the testicular cell suspensions were prepared as described above. The cells were resuspended in 2 mL of PBS containing 5% fetal bovine serum (FBS) and filtered through a 40 μm cell strainer (Corning, 352340). The filtrate was counted and diluted to 1×10^7/mL cells. Then, add Hoechst 33342 (Invitrogen, H3570) at a final concentration of 10 μg/mL and incubate at 32°C for 30 minutes. The cell suspensions were mixed every 5 minutes and kept in the dark to avoid light exposure. After that, the cell suspensions were washed with PBS containing 5% FBS and resuspended in 1 mL PBS containing 5% FBS and 2 μg/mL propidium iodide (Invitrogen, P3566, PI) for 10 minutes. Wash cells in 5 mL PBS containing 5% FBS three times, then centrifuge at 500 g for 3 minutes. Cells were sorted by BD FACSAria Fusion. The gating parameters are referred to the published method and modified according to the actual condition[54]. The sub-populations of spermatogenic cells were collected into 5 mL flow tubes containing 2 mL PBS with 5% FBS. The purity of sorting cells was confirmed by IF with the antibody against SYCP3.

Detect the newly transcribed RNA in spermatocytes

Spermatocytes were collected and cultured in a 6-well culture plate. Add 5-ethynyl-uridine (5-EU) to the culture medium at a final concentration of 1 mM for 2 hours. We also add DMSO as a negative control. After labeling cells with 5-EU, cells were collected and resuspended in PBS, centrifuged at 500 g for 3 min. Cells were fixed with fixation buffer (1% paraformaldehyde, 0.1% TritonX-100, pH 8.2) on the cover glass. The cover glass was placed in humidified chambers at room temperature and air-dried overnight. IF was performed to detect γH2AX as described above. Next, to detect the newly transcribed RNA, we prepared the 500 μL click additive buffer (430 μL click

reaction buffer, 20 μL CuSO4, 1 μL Azide 488, 50 μL click additive, Beyotime, R0301S) for each reaction. The cover glass with cells was placed in a 6-well culture plate and incubated with the click additive buffer for 30 minutes. Then, the click additive buffer was removed. Cells were washed three times with 1 mL PBS containing 3% BSA. Add DAPI and put the cover glass on the glass slide.

RNA extraction and RT-qPCR

Cells were lysed in TRIzol (Invitrogen, 15596018CN) and RNA was extracted according to the standard protocol. Briefly, after different treatments, cells were collected into 1.5 mL tubes (Axygen, MCT-150-C). RNAs were washed with 75% ethanol. For each sample, the extracted RNA was dissolved in 20 μL DEPC water. In order to detect the specific gene expression, we synthesized cDNA with Hifair® AdvanceFast 1st Strand cDNA Synthesis Kit (Yeason, 11149ES60). The products were diluted, and Hieff SYBR Green Master Mix (YEASEN, 11201ES03) was used for qPCR on SIA-PCR007 (Biorad CFX Connect). Primers were designed according to the coding sequences (CCDS) from NCBI using Primer-BLAST and referred to the data from PrimerBank. Cycle threshold (Ct) values were recorded for the analysis. Data were from three technical replicates per sample. Significant differences were identified using Student's t tests.

CUT &Tag assay and analysis

The 1×10^4 spermatocytes were collected for the CUT & Tag assay (Vazyme, TD904) according to the manufacturer's instructions. Briefly, spermatocytes were resuspended in the wash buffer and the nuclei were collected. Then, the nuclei were incubated with ConA Beads for 10 min. The samples were incubated with the primary antibody and

the secondary antibody. pA/G-Tnp transposase was used to cut the genome, and the DNA was extracted and subjected to PCR amplification to build a library. The sequencing process was commissioned by Nanjing Jiangbei New Area Biopharmaceutical Public Service Platform. Following sequencing, raw paired-end reads were subjected to a standardized bioinformatics pipeline for downstream analysis. Initial quality control and adapter trimming were performed to remove low-quality bases. The clean reads were then aligned to the mouse reference genome (mm10) using Bowtie2 (2.3.5.1). Peak calling was conducted with a q-value threshold of 0.05 and different peak analyses with a fold change of RPM >= 2. Alignment files (.bam) were loaded into the Integrative Genomics Viewer (IGV).

Chromatin Isolation by RNA Purification (ChIRP)

ChIRP was carried out as previously described with a few modifications[74]. The pre-rRNA anti-sense oligo probes with 3'-Biotin-TEG modifications were designed by ChIRP Probe Designer (https://www.biosearchtech.com/support/tools/design-software/chirp-probe-designer). Optimize the sonication time (high setting, 30 sec ON and 30 sec OFF, 10 cycles). ChIRP probes were incubated with sonicated chromatin at 37°C for 12 hours with rotation in a molecular hybridization apparatus. The purified DNA was sent to Nanjing Jiangbei New Area Biopharmaceutical Public Service Platform for library preparation and subsequent Illumina HiSeq sequencing.

Assay for Transposase-Accessible Chromatin-sequencing (ATAC-seq)

Spermatocytes were isolated and treated for 12 h with or without BMH-21. Then, pachytene spermatocytes were sorted as described above and lysed in 50 μL lysis buffer (ATAC-seq kit, Vazyme, TD711). Using two replicates per condition, libraries were

prepared using the Hyperactive ATAC-Seq Library Prep Kit for Illumina (Vazyme, TD711) as described with slight modifications[75]. DNA was amplified for 14 cycles and then purified using DNA Clean Beads, followed by elution with 22 μL of nuclease-free water. Finally, the libraries were sent to Nanjing Jiangbei New Area Biopharmaceutical Public Service Platform for sequencing.

In vivo rete testis microinjection of BMH-21

Mice were anesthetized by intraperitoneal administration of Avertin (250 mg kg^{-1}) and positioned supine. Following aseptic preparation, a single incision (~1.5 cm) was made above the genital area, and the testes were exteriorized by gently tractioning the fat pad. BMH-21 (10 μL, 50 μM) or DMSO was injected into the rete testis using a glass capillary under a stereomicroscope. At one-week post-injection, testes were harvested and fixed in 4% paraformaldehyde (PFA) for further analysis.

Quantification and statistical analysis

The areas of different proteins and pre-rRNA were quantified with ImageJ. These quantifications are based on the Analyze module. The main object of observation was selected using the rectangle tool. The fluorescence area and intensity were measured by the Analyze module. Data were collected and analyzed by GraphPad Prism 8. The relative fluorescence intensity data were obtained using ZEN 3.3. An unpaired Student's t-test was used to determine statistical significance, defined as $P < 0.05$.

Data Availability

All datasets have been deposited in the GEO Datasets under the GEO accession

numbers GSE328202, GSE328326, GSE328327, and GSE328328.

Acknowledgements

This work was supported in part by grants from the National Natural Science Foundation of China (32090034), Hangzhou City Leading Innovation and Entrepreneurship Team (TD2020004), "Pioneer" and "Leading Goose" R&D Program of Zhejiang (2024SSYS0033), Westlake Education Foundation, and Westlake Laboratory of Life Sciences and Biomedicine.

Author Contributions

X.Y. designed the project. L.C., X.G., Y.S., P.L., and C.Y. performed the experiments. X.Y. wrote the manuscript. L.C. and X.G. organized figures and edited the manuscript. S.C. and Q. L. analyzed the sequencing data. All authors read and reviewed the manuscript.

Competing interests: The authors declare no competing interests.

References

1. Pederson, T. The plurifunctional nucleolus. *Nucleic Acids Res.* **26**, 3871–3876 (1998).

2. Ferrolino, M. C., Mitrea, D. M., Michael, J. R. & Kriwacki, R. W. Compositional adaptability in NPM1-SURF6 scaffolding networks enabled by dynamic switching of phase separation mechanisms. *Nat. Commun.* **9**, 5064 (2018).

3. Mitrea, D. M. *et al.* Nucleophosmin integrates within the nucleolus via multi-modal interactions with proteins displaying R-rich linear motifs and rRNA. *eLife* **5**, e13571 (2016).

4. Mitrea, D. M. *et al.* Self-interaction of NPM1 modulates multiple mechanisms of liquid-liquid phase separation. *Nat. Commun.* **9**, 842 (2018).

5. Riback, J. A. *et al.* Composition-dependent thermodynamics of intracellular phase separation. *Nature* **581**, 209–214 (2020).

6. Yao, R.-W. *et al.* Nascent Pre-rRNA Sorting via Phase Separation Drives the Assembly of Dense Fibrillar Components in the Human Nucleolus. *Mol. Cell* **76**, 767-783.e11 (2019).

7. Feric, M. *et al.* Coexisting Liquid Phases Underlie Nucleolar Subcompartments. *Cell* **165**, 1686–1697 (2016).

8. Boisvert, F.-M., van Koningsbruggen, S., Navascués, J. & Lamond, A. I. The multifunctional nucleolus. *Nat. Rev. Mol. Cell Biol.* **8**, 574–585 (2007).

9. Barandun, J., Hunziker, M. & Klinge, S. Assembly and structure of the SSU processome-a nucleolar precursor of the small ribosomal subunit. *Curr. Opin. Struct.*

Biol. **49**, 85–93 (2018).

10. Kater, L. *et al.* Visualizing the Assembly Pathway of Nucleolar Pre-60S Ribosomes. *Cell* **171**, 1599-1610.e14 (2017).

11. Singh, S., Vanden Broeck, A., Miller, L., Chaker-Margot, M. & Klinge, S. Nucleolar maturation of the human small subunit processome. *Science* **373**, eabj5338 (2021).

12. Hori, Y., Engel, C. & Kobayashi, T. Regulation of ribosomal RNA gene copy number, transcription and nucleolus organization in eukaryotes. *Nat. Rev. Mol. Cell Biol.* **24**, 414–429 (2023).

13. Leung, A. K. L. *et al.* Quantitative kinetic analysis of nucleolar breakdown and reassembly during mitosis in live human cells. *J. Cell Biol.* **166**, 787–800 (2004).

14. Roussel, P., André, C., Comai, L. & Hernandez-Verdun, D. The rDNA transcription machinery is assembled during mitosis in active NORs and absent in inactive NORs. *J. Cell Biol.* **133**, 235–246 (1996).

15. Dundr, M., Misteli, T. & Olson, M. O. The dynamics of postmitotic reassembly of the nucleolus. *J. Cell Biol.* **150**, 433–446 (2000).

16. Ma, K. *et al.* Ribosomal RNA regulates chromosome clustering during mitosis. *Cell Discov.* **8**, 51 (2022).

17. Sun, S. *et al.* Pre-rRNAs control mitosis by maintaining chromosomal segregation through protecting SMC2 from AURKA-mediated phosphorylation. *Cell Death Dis.* **16**, 812 (2025).

18. Griswold, M. D. Spermatogenesis: The Commitment to Meiosis. *Physiol. Rev.* **96**,

1–17 (2016).

19. de Rooij, D. G. Proliferation and differentiation of spermatogonial stem cells. *Reproduction* **121**, 347–354 (2001).

20. Chen, Y. *et al.* Single-cell RNA-seq uncovers dynamic processes and critical regulators in mouse spermatogenesis. *Cell Res.* **28**, 879–896 (2018).

21. Lake, C. M. & Hawley, R. S. Synaptonemal complex. *Curr. Biol. CB* **31**, R225–R227 (2021).

22. Láscarez-Lagunas, L., Martinez-Garcia, M. & Colaiácovo, M. SnapShot: Meiosis - Prophase I. *Cell* **181**, 1442-1442.e1 (2020).

23. Cesar, B. I. & Kim, Y. Structure and function of the synaptonemal complex. *J. Cell Biol.* **225**, e202511222 (2026).

24. Zheng, Z. *et al.* Reconstitution of SPO11-dependent double-strand break formation. *Nature* **639**, 784–791 (2025).

25. Paiano, J. *et al.* ATM and PRDM9 regulate SPO11-bound recombination intermediates during meiosis. *Nat. Commun.* **11**, 857 (2020).

26. Oger, C. & Claeys Bouuaert, C. SPO11 dimers are sufficient to catalyse DNA double-strand breaks in vitro. *Nature* **639**, 792–799 (2025).

27. Zhang, B., Tang, Z., Li, L. & Lu, L.-Y. NBS1 is required for SPO11-linked DNA double-strand break repair in male meiosis. *Cell Death Differ.* **27**, 2176–2190 (2020).

28. Lu, L.-Y. & Yu, X. Double-strand break repair on sex chromosomes: challenges during male meiotic prophase. *Cell Cycle* **14**, 516–525 (2015).

29. Brick, K., Pratto, F. & Camerini-Otero, R. D. After the break: DSB end processing

in mouse meiosis. *Genes Dev.* **34**, 731–732 (2020).

30. Dereli, I. *et al.* Seeding the meiotic DNA break machinery and initiating recombination on chromosome axes. *Nat. Commun.* **15**, 2941 (2024).

31. Calderón, M. del C., Rey, M.-D., Cabrera, A. & Prieto, P. The subtelomeric region is important for chromosome recognition and pairing during meiosis. *Sci. Rep.* **4**, 6488 (2014).

32. Kauppi, L. *et al.* Distinct properties of the XY pseudoautosomal region crucial for male meiosis. *Science* **331**, 916–920 (2011).

33. Raudsepp, T., Das, P. J., Avila, F. & Chowdhary, B. P. The pseudoautosomal region and sex chromosome aneuploidies in domestic species. *Sex. Dev. Genet. Mol. Biol. Evol. Endocrinol. Embryol. Pathol. Sex Determ. Differ.* **6**, 72–83 (2012).

34. Perry, J., Palmer, S., Gabriel, A. & Ashworth, A. A short pseudoautosomal region in laboratory mice. *Genome Res.* **11**, 1826–1832 (2001).

35. Handel, M. A. The XY body: a specialized meiotic chromatin domain. *Exp. Cell Res.* **296**, 57–63 (2004).

36. Hoyer-Fender, S. Molecular aspects of XY body formation. *Cytogenet. Genome Res.* **103**, 245–255 (2003).

37. Alavattam, K. G., Maezawa, S., Andreassen, P. R. & Namekawa, S. H. Meiotic sex chromosome inactivation and the XY body: a phase separation hypothesis. *Cell. Mol. Life Sci. CMLS* **79**, 18 (2021).

38. Turner, J. M. A. Meiotic sex chromosome inactivation. *Development* **134**, 1823–1831 (2007).

39. Ichijima, Y., Sin, H.-S. & Namekawa, S. H. Sex chromosome inactivation in germ cells: emerging roles of DNA damage response pathways. *Cell. Mol. Life Sci. CMLS* **69**, 2559–2572 (2012).

40. Namekawa, S. H. *et al.* Postmeiotic Sex Chromatin in the Male Germline of Mice. *Curr. Biol.* **16**, 660–667 (2006).

41. Thacker, D., Mohibullah, N., Zhu, X. & Keeney, S. Homologue engagement controls meiotic DNA break number and distribution. *Nature* **510**, 241–246 (2014).

42. Kauppi, L. *et al.* Numerical constraints and feedback control of double-strand breaks in mouse meiosis. *Genes Dev.* **27**, 873–886 (2013).

43. Saldivar, J. C., Cortez, D. & Cimprich, K. A. The essential kinase ATR: ensuring faithful duplication of a challenging genome. *Nat. Rev. Mol. Cell Biol.* **18**, 622–636 (2017).

44. Widger, A. *et al.* ATR is a multifunctional regulator of male mouse meiosis. *Nat. Commun.* **9**, 2621 (2018).

45. Royo, H. *et al.* ATR acts stage specifically to regulate multiple aspects of mammalian meiotic silencing. *Genes Dev.* **27**, 1484–1494 (2013).

46. Ichijima, Y. *et al.* MDC1 directs chromosome-wide silencing of the sex chromosomes in male germ cells. *Genes Dev.* **25**, 959–971 (2011).

47. Lu, L.-Y., Xiong, Y., Kuang, H., Korakavi, G. & Yu, X. Regulation of the DNA damage response on male meiotic sex chromosomes. *Nat. Commun.* **4**, 2105 (2013).

48. Pan, Y.-H. *et al.* Pre-rRNA spatial distribution and functional organization of the nucleolus. *Nature* **646**, 227–235 (2025).

49. Gai, X. *et al.* Pre-ribosomal RNA reorganizes DNA damage repair factors in nucleus during meiotic prophase and DNA damage response. *Cell Res.* **32**, 254–268 (2022).

50. Lafontaine, D. L. J., Riback, J. A., Bascetin, R. & Brangwynne, C. P. The nucleolus as a multiphase liquid condensate. *Nat. Rev. Mol. Cell Biol.* **22**, 165–182 (2021).

51. Riback, J. A. *et al.* Viscoelasticity and advective flow of RNA underlies nucleolar form and function. *Mol. Cell* **83**, 3095-3107.e9 (2023).

52. Bao, X. *et al.* Capturing the interactome of newly transcribed RNA. *Nat. Methods* **15**, 213–220 (2018).

53. Gaysinskaya, V., Soh, I. Y., van der Heijden, G. W. & Bortvin, A. Optimized flow cytometry isolation of murine spermatocytes. *Cytom. Part J. Int. Soc. Anal. Cytol.* **85**, 556–565 (2014).

54. Zou, Q., Yang, L. & Qi, H. Protocol for isolation and proteostatic analysis of sub-populations of spermatogenic cells in mouse. *STAR Protoc.* **3**, 101398 (2022).

55. Pacheco, S. *et al.* ATR is required to complete meiotic recombination in mice. *Nat. Commun.* **9**, 2622 (2018).

56. Widger, A. *et al.* ATR is a multifunctional regulator of male mouse meiosis. *Nat. Commun.* **9**, 2621 (2018).

57. Joshi, N., Brown, M. S., Bishop, D. K. & Börner, G. V. Gradual implementation of the meiotic recombination program via checkpoint pathways controlled by global DSB levels. *Mol. Cell* **57**, 797–811 (2015).

58. Kurzbauer, M.-T., Uanschou, C., Chen, D. & Schlögelhofer, P. The recombinases

DMC1 and RAD51 are functionally and spatially separated during meiosis in Arabidopsis. *Plant Cell* **24**, 2058–2070 (2012).

59. Carpenter, A. T. Recombination nodules and synaptonemal complex in recombination-defective females of Drosophila melanogaster. *Chromosoma* **75**, 259–292 (1979).

60. Abe, H. *et al.* Active DNA damage response signaling initiates and maintains meiotic sex chromosome inactivation. *Nat. Commun.* **13**, 7212 (2022).

61. Peltonen, K. *et al.* A targeting modality for destruction of RNA polymerase I that possesses anticancer activity. *Cancer Cell* **25**, 77–90 (2014).

62. Schier, A. C. & Taatjes, D. J. Structure and mechanism of the RNA polymerase II transcription machinery. *Genes Dev.* **34**, 465–488 (2020).

63. Herman, A. B., Tsitsipatis, D. & Gorospe, M. Integrated lncRNA function upon genomic and epigenomic regulation. *Mol. Cell* **82**, 2252–2266 (2022).

64. Wang, C.-Y., Jégu, T., Chu, H.-P., Oh, H. J. & Lee, J. T. SMCHD1 Merges Chromosome Compartments and Assists Formation of Super-Structures on the Inactive X. *Cell* **174**, 406-421.e25 (2018).

65. Engreitz, J. M. *et al.* The Xist lncRNA exploits three-dimensional genome architecture to spread across the X chromosome. *Science* **341**, 1237973 (2013).

66. Xue, J. *et al.* Visualizing liquid-liquid phase separation and protein aggregates. *Commun. Chem.* **8**, 370 (2025).

67. Brockdorff, N. *et al.* The product of the mouse Xist gene is a 15 kb inactive X-specific transcript containing no conserved ORF and located in the nucleus. *Cell* **71**,

515–526 (1992).

68. Hall, L. L. & Lawrence, J. B. XIST RNA and architecture of the inactive X chromosome: implications for the repeat genome. *Cold Spring Harb. Symp. Quant. Biol.* **75**, 345–356 (2010).

69. Zhang, X. *et al.* Xist in X chromosome inactivation: mechanisms and disease relevance. *Cell Commun. Signal. CCS* **23**, 531 (2025).

70. Dörner, K., Ruggeri, C., Zemp, I. & Kutay, U. Ribosome biogenesis factors-from names to functions. *EMBO J.* **42**, e112699 (2023).

71. Fernandez-Capetillo, O. *et al.* H2AX is required for chromatin remodeling and inactivation of sex chromosomes in male mouse meiosis. *Dev. Cell* **4**, 497–508 (2003).

72. Alavattam, K. G., Abe, H., Sakashita, A. & Namekawa, S. H. Chromosome Spread Analyses of Meiotic Sex Chromosome Inactivation. *Methods Mol. Biol.* **1861**, 113–129 (2018).

73. Namekawa, S. H. Slide preparation method to preserve three-dimensional chromatin architecture of testicular germ cells. *J. Vis. Exp. JoVE* e50819 (2014) doi:10.3791/50819.

74. Sallam, T. *et al.* Transcriptional regulation of macrophage cholesterol efflux and atherogenesis by a long noncoding RNA. *Nat. Med.* **24**, 304–312 (2018).

75. Wu, Z. *et al.* Peripheral nervous system microglia-like cells regulate neuronal soma size throughout evolution. *Cell* **188**, 2159-2174.e15 (2025).

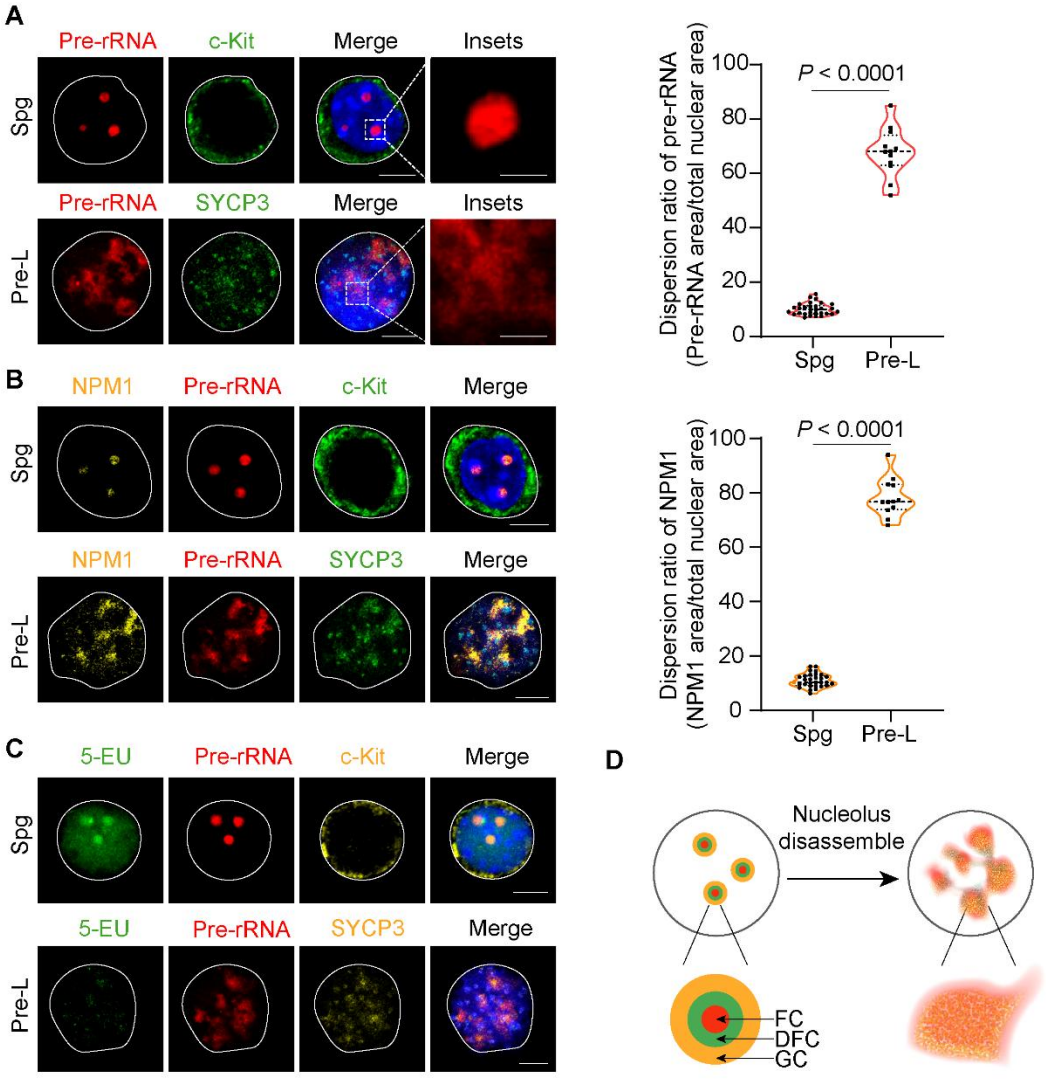

Figure 1 Nucleolus disassembles in the pre-leptotene spermatocytes.

(A) RNA FISH detection of pre-rRNA in spermatogonia (c-Kit+) and pre-leptotene spermatocytes (SYCP3+). Representative images are shown at left. Spg, spermatogonia; Pre-L, pre-leptotene spermatocytes. Quantification of the pre-rRNA dispersion ratio is shown at right.

(B) NPM1 staining in spermatogonia and pre-leptotene spermatocytes. Representative images are shown at left, with quantification of the NPM1 dispersion ratio at right.

(C) Analysis of nascent pre-rRNA synthesis by 5-EU incorporation. Nascent RNA was detected by 5-EU labeling, and total pre-rRNA was visualized by RNA FISH.

(D) Schematic representation of the nucleolar disassembly in the pre-leptotene spermatocytes. The nucleolus is integrity of FC, DFC, and GC in spermatogonia, whereas all three compartments exhibit widespread dispersion throughout the nucleoplasm in the pre-leptotene spermatocytes.

Scale bars, 10 μm.

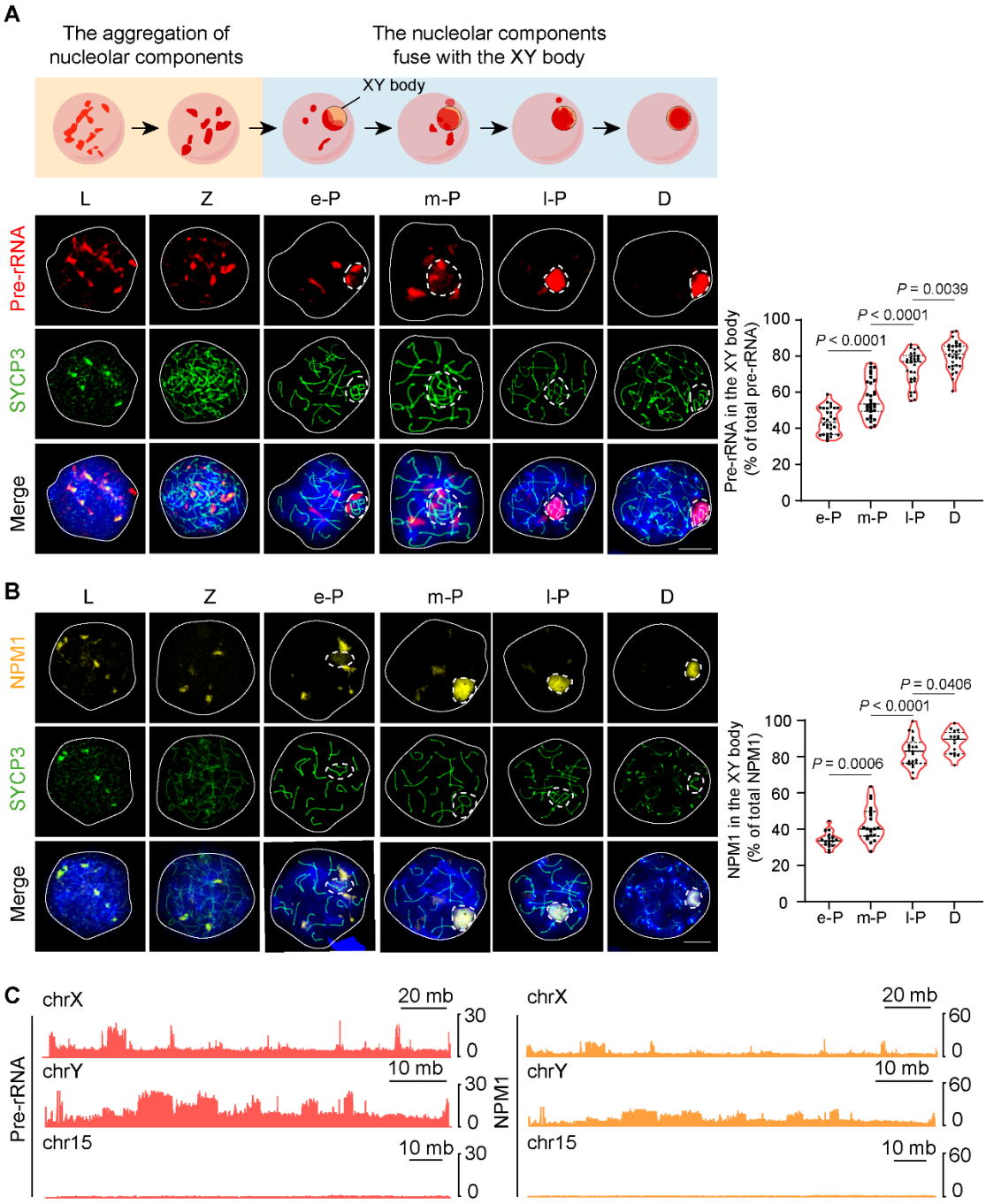

Figure 2 Nucleolar components dynamically fuse with the XY body.

(A) Distribution of pre-rRNA from leptotene to diplotene. Pre-rRNA was detected by RNA-FISH. SYCP3 staining was used to define meiotic stages. A schematic summary is shown at upper left, and representative images are shown below. The XY body is outlined by dashed circles. L, leptotene; Z, zygotene; e-P, early pachytene; m-P, middle pachytene; l-P, late pachytene; D, diplotene. Quantification of pre-rRNA enrichment in

the XY body is shown at right.

(B) Distribution of NPM1 from leptotene to diplotene. Representative images of NPM1 staining are shown at left, with quantification of NPM1 enrichment in the XY body at right.

(C) Pre-rRNA ChIRP-seq and NPM1 CUT&Tag-seq profiles in pachytene spermatocytes.

Scale bars, 10 μm.

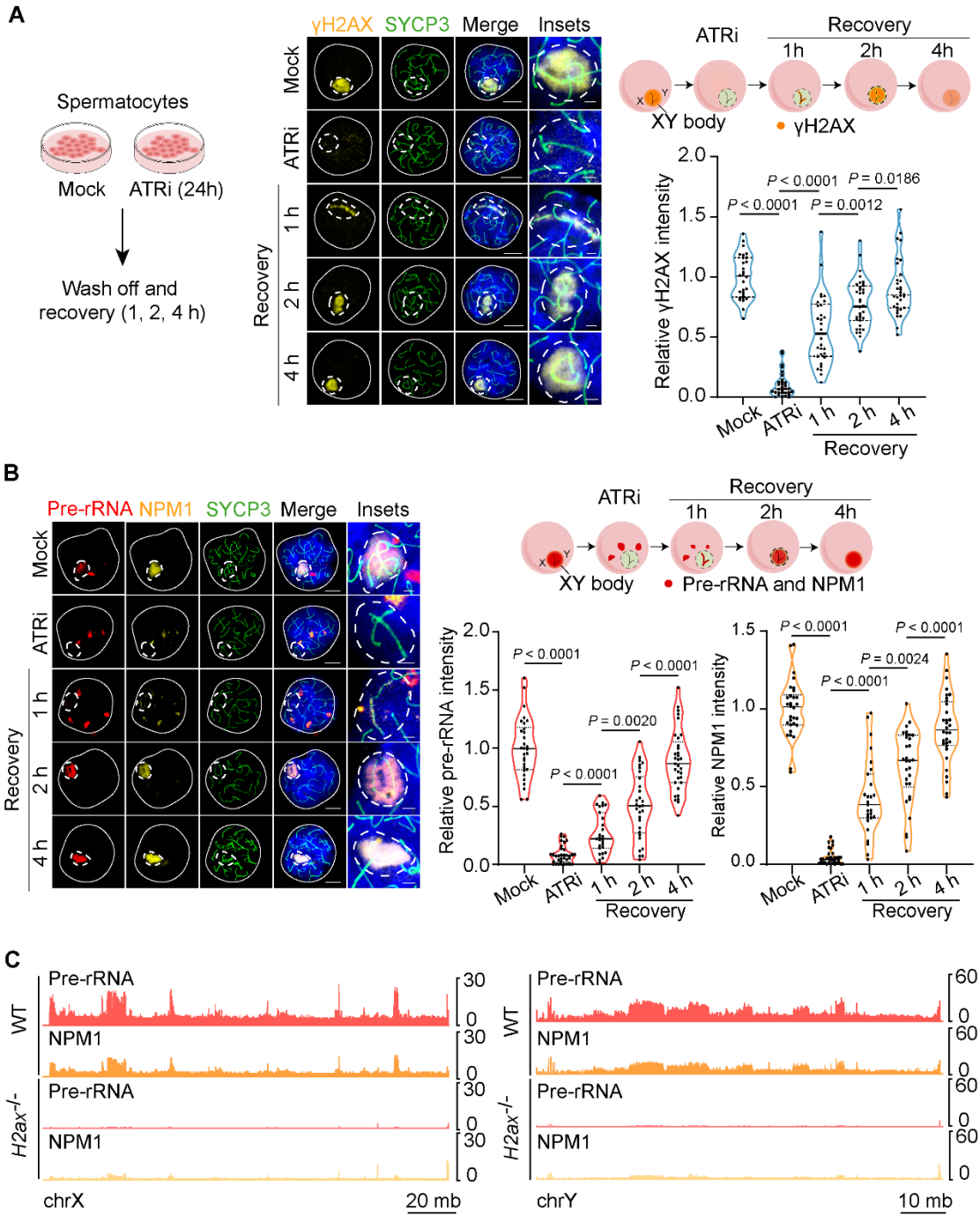

Figure 3 ATR-mediated DNA damage response signaling drives the sequestration of nucleolar components to the XY body.

(A) ATR inhibition and recovery assay in spermatocytes. The spermatocytes were treated with AZ20 (10 μM) for 24 h and collected at the indicated times after washout for immunofluorescence analysis. Representative γH2AX staining images are shown in the middle with a statistical analysis of γH2AX signal in the XY body at lower left. A

schematic summary of γH2AX changes is provided at upper right. The XY body is outlined by dashed circles.

(B) Analysis of pre-rRNA and NPM1 during ATR inhibition and recovery. Representative pre-rRNA and NPM1 staining images are shown at left with a statistical analysis of pre-rRNA and NPM1 signals in the XY body at lower left. A schematic summary of pre-rRNA and NPM1 changes is provided below.

(C) Pre-rRNA ChIRP-seq and NPM1 CUT&Tag-seq profiles on sex chromosomes in WT and *H2ax* KO pachytene spermatocytes.

Scale bars, 10 μm.

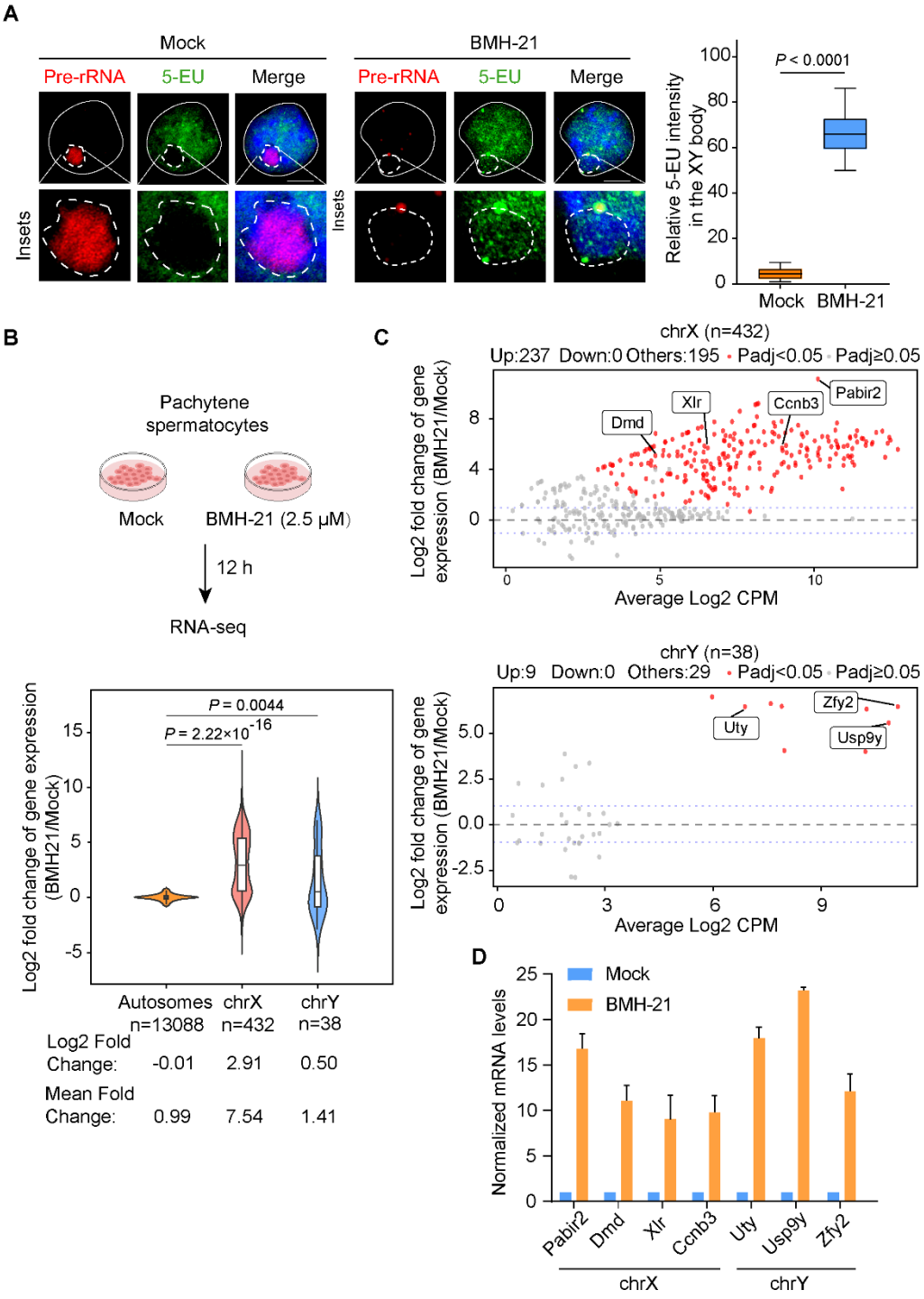

Figure 4 Pre-rRNA mediates MSCI.

(A) BMH-21 releases pre-rRNA from the XY body and promotes nascent RNA production in the XY body. Nascent RNA was measured by 5-EU incorporation. Representative images of pre-rRNA FISH and 5-EU staining are shown at left. The XY body is outlined by dashed circles. Quantification of relative 5-EU intensity in the XY

body is shown at right.

(B) RNA-seq analysis of pachytene spermatocytes treated with BMH-21 (2.5 μM, 12 h). Violin plots show transcriptional changes (BMH-21 versus mock) for autosomal and sex-linked genes.

(C) Scatter plot of differentially expressed sex-chromosomal genes after BMH-21 treatment. Upregulated genes were defined by fold change $\geqslant$ 2 and adjusted $P < 0.05$ (DESeq2).

(D) RT–qPCR validation of representative X- and Y-linked genes upregulated by BMH-21. Data are presented as mean ± s.e.m. (n=3 biological replicates).

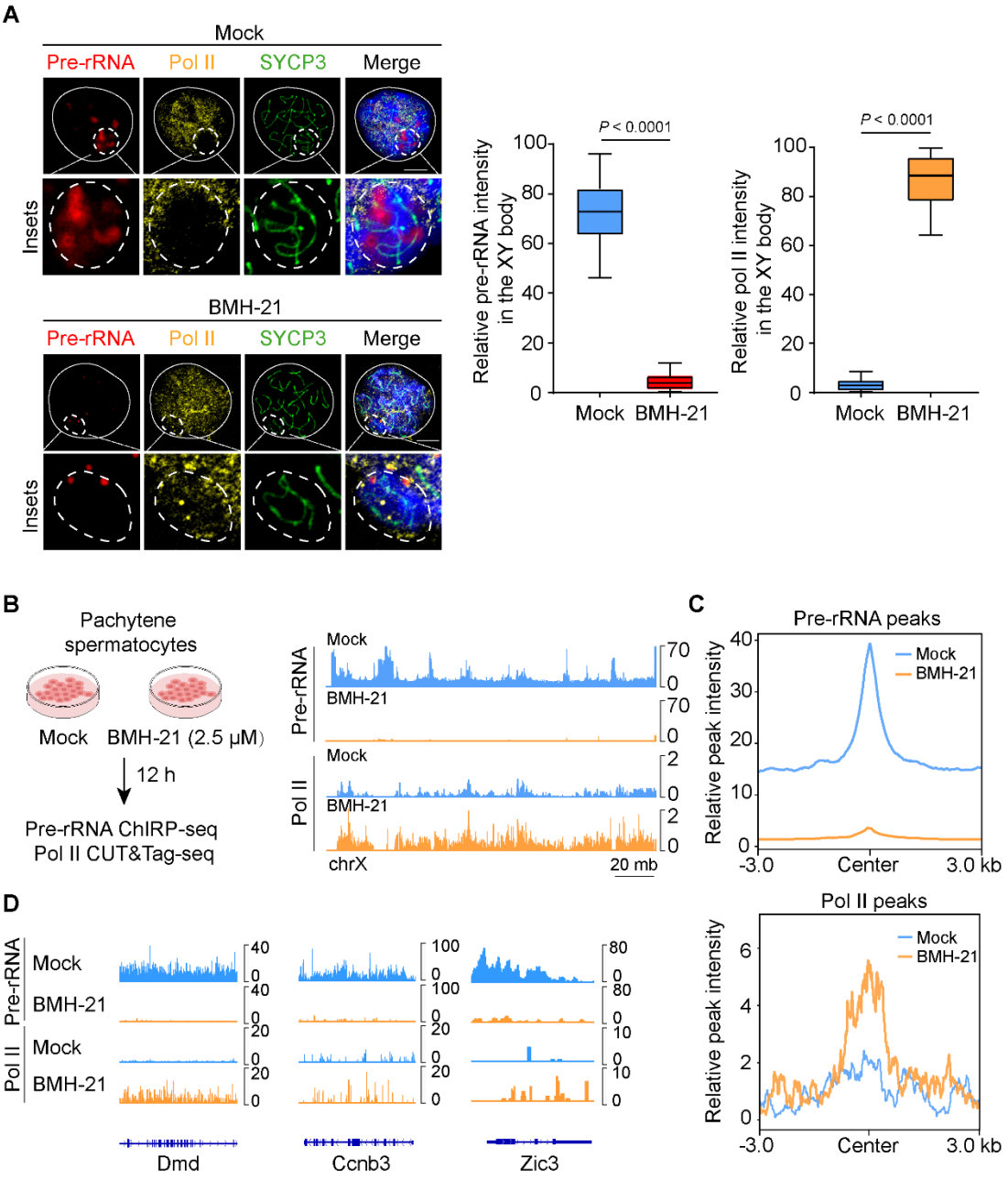

Figure 5 Pre-rRNA excludes RNA Polymerase II from the XY body.

(A) BMH-21 releases pre-rRNA from the XY body and promotes relocalization of Pol II into this compartment. Pachytene spermatocytes were treated with BMH-21 (2.5 μM, 12 h). Pre-rRNA and Pol II were detected by RNA FISH and immunostaining, respectively. Representative images are shown at left, with quantification at right. The XY body is outlined by dashed circles. Scale bar, 10 μm.

(B) Genomic redistribution of pre-rRNA and Pol II after BMH-21 treatment. Pachytene

spermatocytes treated with BMH-21 (2.5 μM, 12 h) were subjected to pre-rRNA ChIRP–seq and Pol II CUT&Tag-seq. Representative profiles across the X chromosome are shown at right.

(C) Metaplot comparison of pre-rRNA ChIRP–seq and Pol II CUT&Tag-seq signals across the sex chromosome.

(D) Representative pre-rRNA ChIRP-seq and RNA Pol II CUT&Tag-seq profiles at X-linked loci.

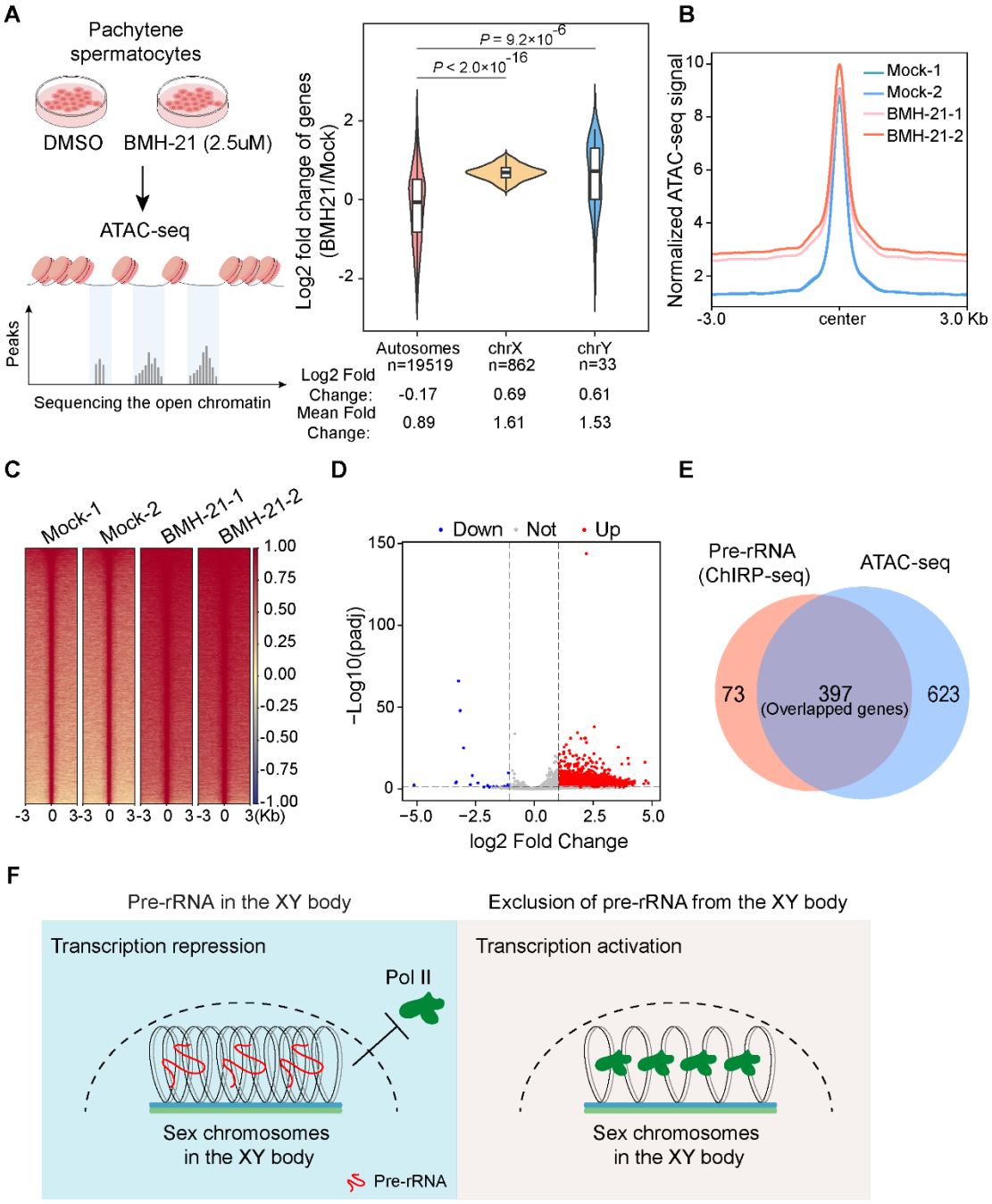

Figure 6 Pre-rRNA enforces a repressive chromatin state in the XY body.

(A) BMH-21 increases chromatin accessibility on the sex chromosomes in pachytene spermatocytes. Chromatin accessibility was assessed by ATAC-seq after BMH-21 treatment (2.5 μM, 12 h). Violin plots show ATAC-seq changes (BMH-21 versus mock) across autosomes and sex chromosomes.

(B) Metaplot comparison of ATAC-seq signals across the sex chromosomes.

(C) Heat map of ATAC-seq signals across the sex chromosomes.

(D) Scatter plot of sex-chromosomal genes with significantly altered chromatin accessibility after BMH-21 treatment.

(E) Overlap between sex-linked genes with increased chromatin accessibility by ATAC-seq and reduced pre-rRNA occupancy by ChIRP-seq after BMH-21 treatment.

(F) Working model of pre-rRNA-mediated MCSI. In the XY body, pre-rRNA restricts chromatin accessibility and excludes RNA polymerase II, thereby maintaining transcription repression in the sex chromosomes.